Cerebral amyloid angiopathy-linked β-amyloid mutations promote cerebral fibrin deposits via increased binding affinity for fibrinogen

Steven A. Cajamarca[a], Erin H. Norris[a], Louise van der Weerd[b,c], Sidney Strickland[a], and Hyung Jin Ahn[d,e,1]

[a]Patricia and John Rosenwald Laboratory of Neurobiology and Genetics, The Rockefeller University, New York, NY 10065; [b]Department of Radiology, Leiden University Medical Center, 2333 ZA Leiden, The Netherlands; [c]Department of Human Genetics, Leiden University Medical Center, 2300 RC Leiden, The Netherlands; [d]Department of Pharmacology, Physiology and Neuroscience, Rutgers–New Jersey Medical School, Newark, NJ 07101; and [e]Brain Health Institute, Rutgers University, Piscataway, NJ 08854

Edited by Gregory A. Petsko, Brigham and Women's Hospital, Boston, MA, and approved May 1, 2020 (received for review December 4, 2019)

Cerebral amyloid angiopathy (CAA), where beta-amyloid (Aβ) deposits around cerebral blood vessels, is a major contributor of vascular dysfunction in Alzheimer's disease (AD) patients. However, the molecular mechanism underlying CAA formation and CAA-induced cerebrovascular pathology is unclear. Hereditary cerebral amyloid angiopathy (HCAA) is a rare familial form of CAA in which mutations within the (Aβ) peptide cause an increase in vascular deposits. Since the interaction between Aβ and fibrinogen increases CAA and plays an important role in cerebrovascular damage in AD, we investigated the role of the Aβ–fibrinogen interaction in HCAA pathology. Our work revealed the most common forms of HCAA-linked mutations, Dutch (E22Q) and Iowa (D23N), resulted in up to a 50-fold stronger binding affinity of Aβ for fibrinogen. In addition, the stronger interaction between fibrinogen and mutant Aβs led to a dramatic perturbation of clot structure and delayed fibrinolysis. Immunofluorescence analysis of the occipital cortex showed an increase of fibrin(ogen)/Aβ codeposition, as well as fibrin deposits in HCAA patients, compared to early-onset AD patients and nondemented individuals. Our results suggest the HCAA-type Dutch and Iowa mutations increase the interaction between fibrinogen and Aβ, which might be central to cerebrovascular pathologies observed in HCAA.

hereditary cerebral amyloid angiopathy | fibrinogen | β-amyloid | fibrinolysis

Most Alzheimer's disease (AD) patients suffer from cerebrovascular pathologies, such as altered cerebral blood flow and a damaged cerebral vasculature (1, 2). Furthermore, some cerebrovascular symptoms, including white matter hyperintensity, are very early pathologies in AD (3, 4). Cerebral amyloid angiopathy (CAA), which results from β-amyloid (Aβ) deposits around cerebral blood vessels, is observed in more than 80% of AD patients (2, 5). Examination of brain pathology in AD patients suggests that CAA is a major contributor of cerebrovascular pathologies in AD, including loss of smooth muscle cells, perivascular microhemorrhage, microinfarctions, and capillary occlusion (2, 5, 6). However, the details of how CAA contributes to vascular dysfunction in AD is unclear.

While CAA is mostly observed in the sporadic form of AD patients in late adulthood, rare familial forms occur in midadulthood and lead to more severe cerebrovascular disease, including severe strokes, early onset dementia, and ultimately death (7–9). Although most AD-linked amyloid precursor protein (APP) mutations elevate total Aβ production or promote formation of the more toxic Aβ42, a subset of mutations related to hereditary cerebral amyloid angiopathy (HCAA) cause a dramatic increase in vascular deposits of Aβ. Since patients afflicted by HCAA mutations have severe cerebrovascular disorders along with the presence of severe CAA pathology in their midlife (9), HCAA is an ideal disease to examine the pathogenic mechanisms of CAA. The most common forms of HCAA result from the Dutch mutation (E22Q). However, several other HCAA mutations, such as Iowa (D23N) and Italian (E22K) mutations, have been identified. Most APP mutations involved in HCAA are clustered in the amino acid 21 to 23 region of Aβ (9, 10). Why mutations specifically in this region of Aβ increase vascular amyloid deposits, but do not increase parenchymal Aβ plaques, is not yet clear although it suggests that this region plays a role in Aβ's deposition in the vasculature.

Accumulating evidence implicates fibrin(ogen), the main protein component of blood clots, in AD pathogenesis (11–13). Soluble fibrinogen is converted into fibrin through activation of the coagulation cascade, which normally serves a beneficial hemostatic role. However, persistent fibrin deposited on cerebral vessel walls can lead to vessel occlusions and brain parenchymal ischemia (12, 14). Fibrinogen binds to Aβ42, which leads to the formation of structurally abnormal fibrin clots that are more resistant to fibrinolysis than normal clots (15–17). Fibrinogen binding to Aβ also promotes Aβ aggregation in vitro and contributes to the development of CAA in AD mouse models (11, 12, 15, 18). In addition, fibrin(ogen) colocalizes with Aβ along cerebral vessel walls in AD patients and AD mouse models (12, 18). Furthermore, analysis of the fibrinogen-binding region of Aβ42 indicates this region overlaps with Aβ sites that are mutated in various HCAA-disease variants (amino acids 21 to 23), including amino acid 22 in HCAA-Dutch, -Arctic, and -Italian, and amino acid 23 in HCAA-Iowa (9, 10). Thus, we hypothesized the interaction between HCAA Aβ and fibrinogen may have a role in the development of exacerbated CAA pathology observed in HCAA patients. While the Aβ40:Aβ42 ratio is elevated in CAA, Aβ42 is still a major

Significance

We found an increased interaction between CAA-linked mutant Aβ and fibrin(ogen) that may not only result in severely altered fibrin structure and function but may also lead to vast amounts of fibrin(ogen)/Aβ codeposition, as well as fibrin deposits in HCAA patients. This finding provides a molecular mechanism for how CAA-linked mutations may lead to severe cerebrovascular pathology in HCAA patients by enhancing the protein–protein interaction.

Author contributions: S.A.C., S.S., and H.J.A. designed research; S.A.C. and H.J.A. performed research; S.A.C., E.H.N., S.S., and H.J.A. analyzed data; and S.A.C., E.H.N., L.v.d.W., S.S., and H.J.A. wrote the paper.

The authors declare no competing interest.

This article is a PNAS Direct Submission.

[1]To whom correspondence may be addressed. Email: hyungjin.ahn@rutgers.edu.

This article contains supporting information online at https://www.pnas.org/lookup/suppl/doi:10.1073/pnas.1921327117/-/DCSupplemental.

component of CAA deposits (19). Therefore, we investigated both Aβ40 and Aβ42 peptides.

Results

HCAA-Type Dutch and Iowa Mutations Increase Aβ's Binding Affinity for Fibrinogen. Previously, our biochemical analysis revealed that the central region of Aβ42, including amino acids 17 to 23, is critical to its interaction with fibrinogen (17). To investigate how single amino acid mutations in this region of Aβ42 affect binding affinity for fibrinogen, we synthesized four biotinylated alanine-scanning peptide Aβ fragment analogs (L17A, E22A, D23A, and V24A) and analyzed their binding for fibrinogen using AlphaLISA. E22A and D23A mutants demonstrated up to 40 times stronger binding to fibrinogen than wild-type (WT) Aβ42 while L17A and V24A mutants showed similar binding affinities for fibrinogen comparable to WT Aβ42 (Fig. 1*A*). These results suggested that mutations in Aβ sites commonly found in HCAA disease (amino acids 22 and 23) significantly increase Aβ's binding affinity for fibrinogen and warranted further examination to see if HCAA-type Aβs, specifically Iowa (D23N) and Dutch (E22Q) Aβ, interact with fibrinogen differently compared to WT Aβ.

To determine specific binding affinity of HCAA-type Aβ mutants for fibrinogen, we compared the interaction between the various Aβ peptides and fibrinogen using surface plasmon resonance (SPR) (Fig. 1 *B–I*). We immobilized biotinylated fibrinogen on an Avidin immobilized ProteOnNLC sensor chip and infused various concentrations of oligomeric WT, Iowa (D23N), or Dutch (E22Q) Aβ42 or Aβ40, in a dose-dependent manner, into the chip for 2 min (Fig. 1 *D–I*). Equilibrium dissociation constants (K_Ds) (Fig. 1 *B* and *C*) were calculated from association (k_a) and dissociation (k_d) rate constants for the complex generated from every association (from 0 to 120 s) and dissociation (120 to 10,000 s) event between the different Aβ42 (Fig. 1 *D–F*) or Aβ40 (Fig. 1 *G–I*) peptides and fibrinogen. Dutch and Iowa Aβ42 (Dutch42 and Iowa42) peptides

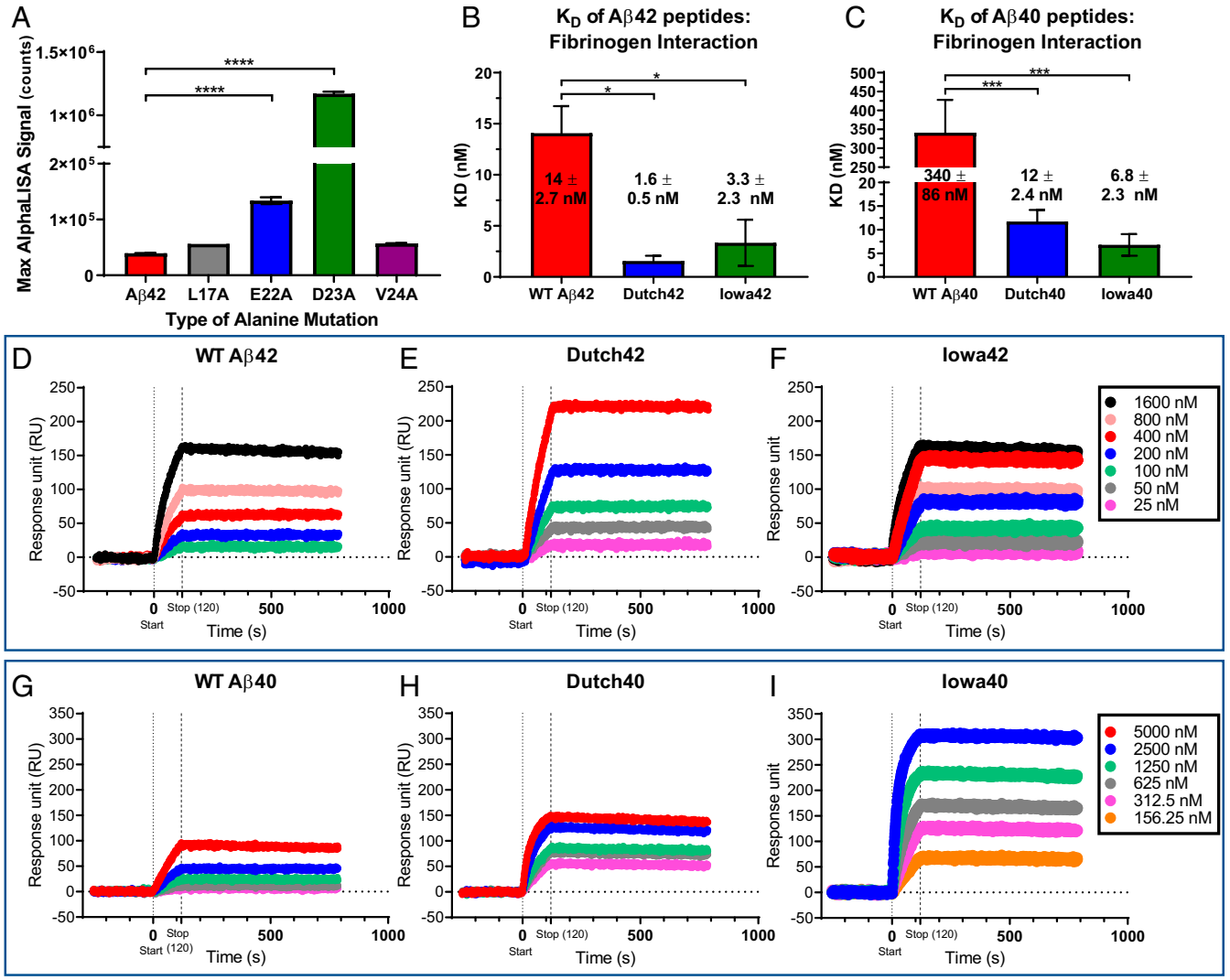

Fig. 1. HCAA-type mutations increase Aβ's binding affinity for fibrinogen. (*A*) AlphaLISA binding assay was performed using human purified fibrinogen and various concentrations of biotinylated alanine-scanning peptide analogs of Aβ42 (L17A, E22A, D23A, and V24A). The bar graph indicates the maximum binding between fibrinogen and the various Aβ fragments and WT Aβ42. Alanine mutations in amino acid positions 22 and 23 vastly increased Aβ's binding to fibrinogen compared to WT Aβ42 (red bar) and other alanine-scanning analogs (****$P < 0.0001$; $n = 3$–6 per group). (*B* and *C*) Bar graphs generated from SPR curves show that the K_D of fibrinogen binding of HCAA-type Aβ42 (*B*) and Aβ40 (*C*) is stronger than the binding affinity of their WT Aβ counterparts. (***$P < 0.001$; *$P < 0.05$. $n = 3$–6). Bar graphs represent mean ± SEM of ≥3 separate experiments. (*D–I*) Representative SPR response curves of WT, Dutch, and Iowa Aβ42 (*D–F*) and Aβ40 (*G–I*) peptides, respectively, that were infused over immobilized fibrinogen indicate that HCAA Aβ exhibited higher SPR association response signal compared to WT Aβ. Statistical analyses were performed using one-way ANOVA followed by Tukey's post hoc test.

had lower K_D values with fibrinogen compared to WT Aβ42, indicating approximately four to eight times stronger binding affinity (Fig. 1*B*). Dutch and Iowa Aβ40 (Dutch40 and Iowa40) peptides had ∼30 to 50 times stronger binding affinity to fibrinogen compared to WT Aβ40 (Fig. 1*C*). Overall, HCAA-Aβ peptides revealed a stronger binding interaction with fibrinogen compared to their respective WT Aβ counterparts. To determine if the interaction to fibrinogen was specific to Aβ, we immobilized biotinylated bovine serum albumin (BSA) and infused the different Aβ peptides over the sensor chip and found no interaction (*SI Appendix*, Fig. S1*A*). In addition, to analyze whether another amyloidogenic protein could interact with fibrinogen, we infused amylin at similar concentrations as the Aβ peptides over immobilized fibrinogen but did not observe any interaction (*SI Appendix*, Fig. S1*B*). These results suggest the HCAA-type single amino acid mutations increase Aβ's binding affinity for fibrinogen.

The aggregated state and solubility of Aβ is important in driving Aβ deposition in AD brains (20, 21) where soluble oligomeric Aβ is thought to be the primary toxic species. Oligomeric WT Aβ42 has a higher binding affinity to fibrinogen compared to WT Aβ40 (15), possibly due to Aβ42's higher aggregation propensity. HCAA Aβs are highly prone to self-aggregation (22–24), which could explain their observed higher binding affinity to fibrinogen compared to WT Aβ42. To assess the aggregation state of the WT and HCAA Aβ42 and Aβ40 peptides used for our in vitro experiments, we viewed each peptide via transmission electron microcopy (TEM) (*SI Appendix*, Fig. S2). Compared to WT Aβ42/40 (*SI Appendix*, Fig. S2 *A* and *D*), Dutch42/40 (*SI Appendix*, Fig. S2 *B* and *E*) and Iowa42/40 (*SI Appendix*, Fig. S2 *C* and *F*) peptides oligomerized to a greater extent, forming larger oligomers and protofibrils. These results indicate that the mutant HCAA Aβs used in our in vitro experiments are more aggregated, which can have a meaningful impact on fibrin(ogen) binding.

To further understand whether the aggregation state of Aβ could affect the binding affinity to fibrinogen, we compared the aggregation state of WT Aβ42 incubated overnight (*SI Appendix*, Fig. S3*A*) to WT Aβ42 incubated at 4 °C for 7 d (*SI Appendix*, Fig. S3*B*) to induce a more aggregated state with more protofibrils and fibrils. We performed binding SPR experiments with immobilized fibrinogen (*SI Appendix*, Fig. S3*C*) using the 7-d-incubated WT Aβ42 peptide. Both 1- and 7-d incubations of WT Aβ42 exhibited similar K_D values, 14 ± 2.7 nM and 12 ± 7.8 nM, respectively. Thus, the more aggregated state of WT Aβ42 did not affect the binding affinity to fibrinogen (*SI Appendix*, Fig. S3*D*). These results indicate that the aggregation state of Aβ alone does not dictate its binding affinity to fibrinogen. Other factors, such as changes to the physicochemical properties of Aβ due to the HCAA mutations, may be significantly contributing to the strong binding affinity in Aβ-fibrinogen (fbg) interaction.

Alterations to Fibrin Clot Architecture Induced by HCAA Aβ Compared to WT Aβ. Given that WT Aβ42 leads to an altered fibrin architecture (18), the stronger interaction between HCAA Aβ and fibrinogen (Fig. 1) may have further aggravating effects on fibrin clot structure. To determine the structural effects of HCAA Aβ on in vitro fibrin clot formation, clots were formed using purified human fibrinogen in the absence of Aβ (Fig. 2*A*) or incubated with the Aβ42 peptides (Fig. 2 *B–D*) and the Aβ40 peptides (Fig. 2 *E–G*) (18). Fig. 2 shows representative scanning electron microscope (ScEM) images of the various clots (Fig. 2 *A–G*) that were acquired and analyzed for fiber thickness (Fig. 2 *H* and *I*) and number of aggregated clot aggregates or clumps (Fig. 2 *J* and *K*). Normal fibrin clots incubated in the absence of Aβ (Fig. 2*A*) demonstrated a homogenous area of normal clot mesh consisting of fibrin fibers that averaged 84 ± 3.0 nm (mean ± SEM) in thickness and revealed nearly no amorphous clumps or fiber aggregates. When clots were formed in the presence of WT Aβ42 (Fig. 2*B*), thinner clot fibers formed with a mean thickness of 56 ± 2.0 nm along with the presence of aggregated fibrin clumps (indicated by the red asterisks in Fig. 2*B*), as previously reported (16, 18, 25). Compared to WT Aβ42, fibrin clots in the presence of Dutch Aβ42 (Fig. 2*C*) showed signs of greater alteration to the fibrin network, with thinner fibers with a mean thickness of 40 ± 1.5 nm (Fig. 2*H*) and more aggregates compared to WT Aβ42 (Fig. 2*J*), while Iowa Aβ42 (Fig. 2*D*) led to even thinner fibers, with a mean thickness of 33 ± 1.1 nm and an increased trend of fibrin clumps (Fig. 2*J*). HCAA mutant Aβ40 peptides also led to more dramatic structural changes to fibrin clot fibers compared to their WT Aβ40 counterpart (Fig. 2*E*). Fibrin fibers formed in the presence of Dutch (Fig. 2*F*) or Iowa Aβ40 (Fig. 2*G*) were thinner and more tortuous (mean fiber thickness of 29 ± 1.0 nm and 57± 2.5nm, respectively) (Fig. 2*I*), with more fiber clumps (Fig. 2*K*). WT Aβ40-induced clots did not lead to structural changes to clot formation compared to fibrin clots formed in the absence of Aβ, which correlates with its weaker binding affinity to fibrinogen, K_D of 340 ± 86 nM, in SPR analysis (Fig. 1*C*). These results indicate that the Dutch and Iowa HCAA Aβ mutations enhance Aβ's perturbation of fibrin clots, which was especially dramatic with the Aβ40 peptides. Thus, the alterations of HCAA Aβs to clot architecture correlate with their stronger fibrinogen binding affinity.

To test the possibility if lower HCAA Aβ concentrations could have meaningful effects on fibrin clot structure, we made fibrin clots with lower concentrations of WT and HCAA mutant Aβ (375 nM). The fibrinogen concentration in these clots was lowered to 1 μM, which is the minimum concentration at which clots can be formed on glass slides for ScEM imaging. Since perturbations in clot lysis is Aβ concentration-dependent, where an Aβ concentration higher than a 1:3 Aβ:fbg molar ratio is necessary to show the effects of Aβ in clot formation and dissolution (16), we made clots in 375 nM Aβ. The qualitative gross effects of lower levels of Dutch42 (*SI Appendix*, Fig. S4*C*) and Iowa42 (*SI Appendix*, Fig. S4*D*) Aβ on fibrin fiber structure were still evident, with a fibrin mesh that is more irregular and aggregated compared to the WT Aβ42-induced fibrin mesh (*SI Appendix*, Fig. S4*B*). However, the effects were less severe at this lower HCAA Aβ concentration. These results suggest that lower Aβ concentrations still exhibit clear differences on fibrin clots between WT and HCAA Aβs.

HCAA-Type Aβs Increase Resistance to Fibrinolysis Compared to WT Aβ. Since the Aβ–fibrinogen interaction is known to delay plasmin-mediated fibrinolysis (16), we tested whether the stronger interactions with fibrinogen shown by the HCAA-type Aβ peptides translated into functional consequences in clot formation and dissolution (fibrinolysis) using an in vitro clot turbidity assay (Fig. 3). Turbidity assays can monitor the kinetics of the clotting process by measuring the turbidity of a solution as it increases during clot formation and decreases during clot dissolution or fibrinolysis. Fibrinolysis of the fibrin clot in the presence of Aβ42 was delayed (red line curve, Fig. 3*A*) relative to the buffer control clot made without Aβ peptide (black line curve, Fig. 3*A*), as previously reported (11, 16), also depicted as an increase in time to half lysis (Fig. 3*C*). Fibrinolysis was further delayed in the presence of Iowa-type Aβ42 (gray line curve, Fig. 3*A*) relative to WT Aβ42 (red line curve, Fig. 3*A*), which resulted in a prolonged time to half lysis for Iowa42 relative to WT Aβ42 (Fig. 3*C*). Under the same conditions, fibrin clot formation and dissolution in the presence of WT Aβ40 (red line curve, Fig. 3*B*) showed similar kinetics to that of control buffer (black line curve, Fig. 3*B*); however, fibrin clots formed in the presence of Dutch Aβ40 and Iowa Aβ40 (green and gray line curves, respectively, in Fig. 3*B*) prolonged fibrinolysis and led to an increase in time to half lysis compared to WT Aβ40 (Fig. 3*D*). These results were consistent with our ScEM images (Fig. 2) in which the HCAA Aβ-induced clots were more structurally altered compared to WT Aβ-induced

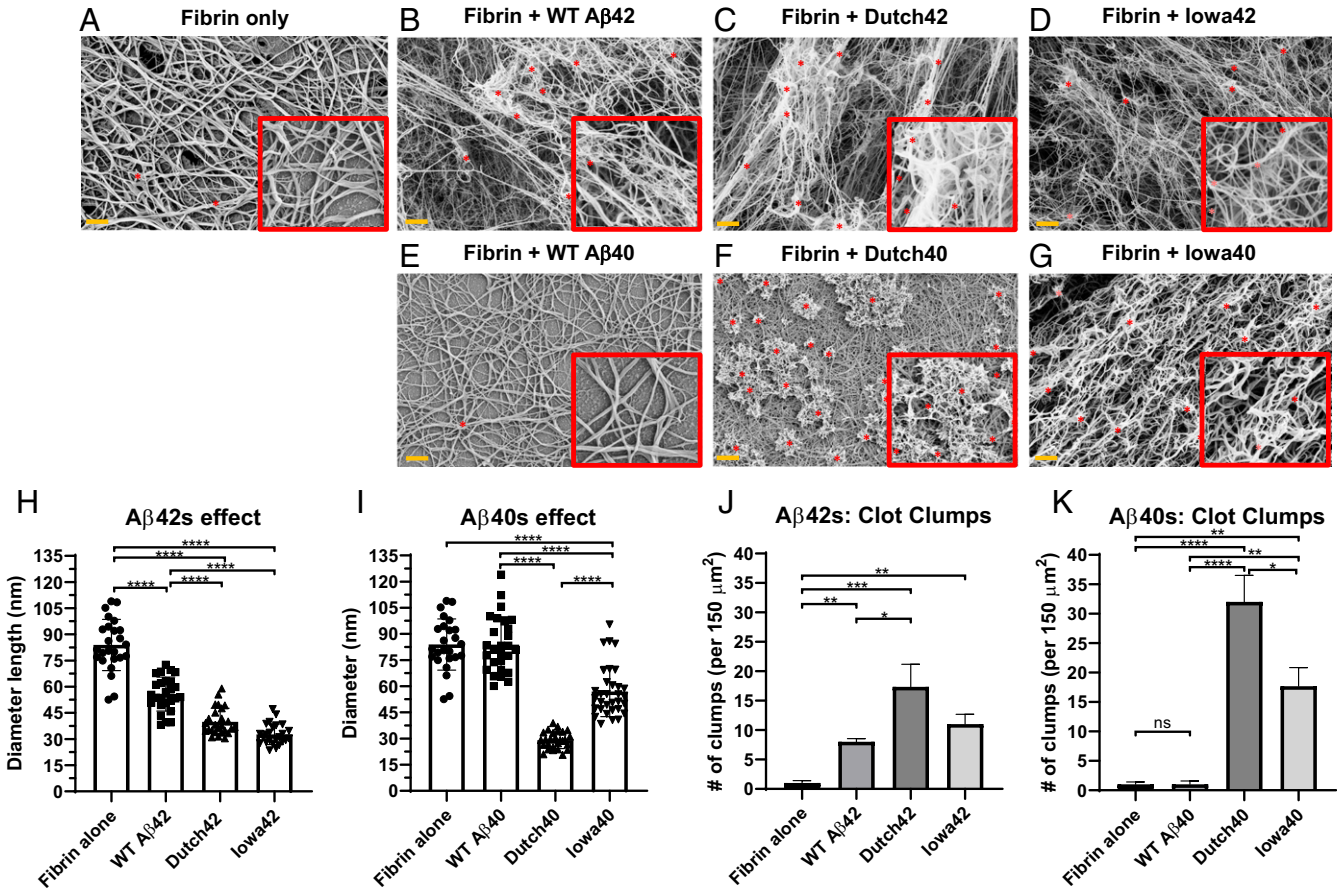

Fig. 2. HCAA Aβ-induced fibrin clots demonstrate greater structural alterations than WT Aβ-induced clots. ScEM analysis of clots formed in the presence of (*A*) no Aβ (control), (*B*) WT Aβ42, (*C*) Dutch Aβ42, (*D*) Iowa Aβ42, (*E*) WT Aβ40, (*F*) Dutch Aβ40, and (*G*) Iowa Aβ40. Fibrin clots were prepared using human fibrinogen (1.5 μM), in the absence or presence of Aβ peptides (3.0 μM). (*H–K*) Quantification of clot fiber diameter (nm) and number of aggregates/clumps. (*H* and *J*) HCAA Aβ42-induced clots show greater alteration in fibrin clot structure with thinner fibers and clumps compared to WT Aβ42. (*I* and *K*) HCAA Aβ40-induced clots also led to fibrin clot with a smaller fiber diameter and increased clumps relative to WT Aβ40. Uniquely, WT Aβ40 did not have gross effect on fibrin structure (*E*), fiber thickness (*I*), and aggregates (*K*) compared to control clots made without Aβ (*A*). Red box *Insets* display clots at 2.3 times higher magnification. Red asterisks (*) on clot images are indicative of some of the fibrin aggregates/clumps counted per clot. Bar graphs represent mean ± SEM of ≥3 separate images per clot. Statistical analyses were performed using one-way ANOVA followed by Tukey's post hoc test. ****$P < 0.0001$; ***$P < 0.001$; **$P < 0.01$; *$P < 0.05$. ns (not significant) = $P > 0.05$. Clots visualized via ScEM are representative of ≥3 separate experiments. (Orange scale bar: 1 μm.)

clots. These findings suggest that HCAA-type Aβs not only alter the fibrin network architecture, but also have a greater functional impact on the clotting clearance process compared to WT Aβ.

Increased Vascular Aβ and Fibrino(gen) Codeposition in HCAA Patients' Cortex Blood Vessel Walls. The stronger binding affinity for fibrinogen and delayed fibrinolysis by HCAA Aβs (Fig. 1) could translate to higher levels of fibrin(ogen) deposits at sites of CAA in HCAA patients' brains. To test this hypothesis, we acquired postmortem human occipital cortex brain tissue from HCAA-Dutch ($n = 5$) and -Iowa ($n = 1$) type patients, age-matched non-HCAA, early-onset AD (EOAD) patients ($n = 5$), and nondementia (ND) controls ($n = 7$) (*SI Appendix*, Table S1) (of note, EOAD patients collected for our analysis do not contain any mutation within Aβ or near Aβ cleavage sites as confirmed by sequencing of exon 16 and 17 of the *APP* gene). Using these tissues, we probed for fibrin(ogen) deposits (Dako antibody) and congophillic aggregated Aβ deposits (Congo Red) and assessed their colocalization via immunofluorescence (IF) analysis (Fig. 4). We imaged a single HCAA-Iowa patient's brain due to the limited number of HCAA-Iowa cases and did not include it into our quantification analysis. Consistent with previous findings (12, 18), our IF analysis showed that EOAD brains overall contained higher fibrin(ogen) deposition than ND brains (Fig. 4*A*). They had elevated fibrin(ogen) deposition (Fig. 4*B*) in and around vascular sites, often at sites of CAA-laden parenchymal vessels, which was pervasive throughout the EOAD occipital cortex samples (as depicted in Fig. 4*A*, cyan, vascular Aβ deposits). HCAA-Dutch and -Iowa type patients showed more fibrin(ogen) staining, especially in and around CAA-laden vessels compared to EOAD and ND brains (Fig. 4 *A* and *B*). While HCAA-Dutch brains had an elevated amount of vascular Aβ deposits with increased sites of CAA, EOAD brains often presented with abundant CAA pathology and Aβ parenchymal plaques, which made our analysis of total Aβ deposits (Fig. 4*C*) reveal no difference between HCAA-Dutch and EOAD brains.

While EOAD brains contained a considerable amount of CAA pathology, confocal microscopy analysis showed that there was higher fibrin(ogen) colocalization with Aβ deposits in HCAA brains compared to EOAD brains (Fig. 4*D*), at sites of parenchymal Aβ plaques, and especially striking at sites of CAA pathology. Aβ deposits and fibrin(ogen) codeposition was depicted as an overlapping merged channel (Fig. 4*A*, merged, yellow). Closer examination of Congo Red-positive (+) (CAA-laden) vessels, specifically, among the groups also revealed much higher levels of intravascular and extravascular fibrin(ogen) codeposition with congophillic Aβ

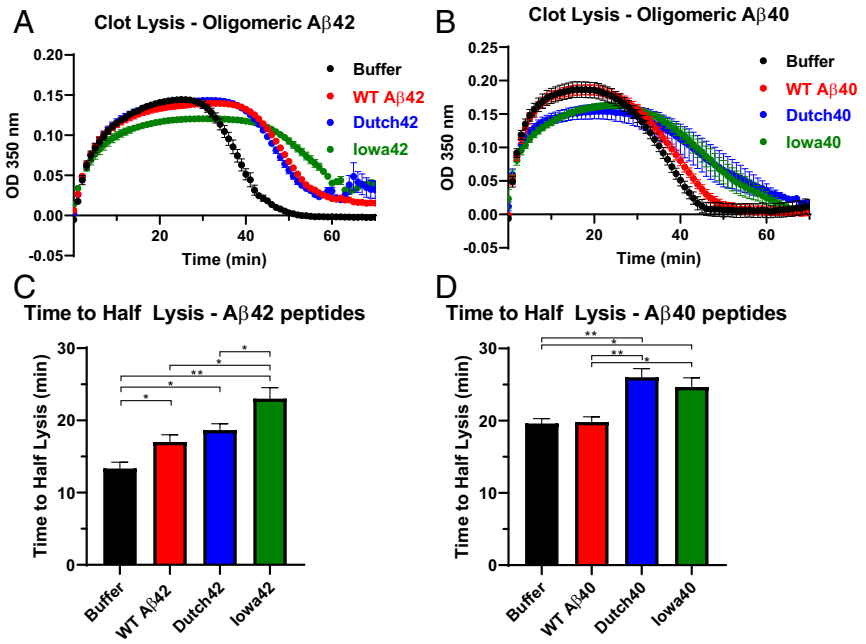

Fig. 3. HCAA-type Aβs increase resistance to fibrinolysis compared to WT Aβ. (*A* and *B*) Fibrin clot formation and degradation were assessed by measuring time-dependent turbidity changes at 350 nm. These experiments involved incubation of fibrinogen, tPA, plasminogen, and the absence (black, buffer control only) or presence of WT Aβ (red) or HCAA Aβ peptides (blue for Dutch, green for Iowa). Reactions were initiated by adding thrombin. Time-dependent turbidity plots show the effect of WT Aβ42 and HCAA Aβ42 (*A*) and WT Aβ40 and HCAA Aβ40 (*B*) on thrombosis and fibrinolysis. (*C*) Time to half-lysis times for WT Aβ42, Dutch42, and Iowa42 are prolonged compared to control. Clot lysis time of Iowa42 was significantly more delayed than WT Aβ42. (**$P < 0.01$; *$P < 0.05$; $n = 3$). (*D*) While WT Aβ40 did not have any effect on fibrin clot lysis, Dutch40 and Iowa40 significantly delayed fibrinolysis compared to buffer alone and WT Aβ40. (**$P < 0.01$; *$P < 0.05$; $n = 3$). Statistical analyses were performed using one-way ANOVA followed by Tukey's post hoc test. Bar graphs represent mean ± SEM of ≥3 separate experiments.

in the HCAA brains (Fig. 4*E*). These results suggest that there is more interaction between HCAA Aβ and fibrin(ogen) in CAA-laden vessels compared to EOAD patients who also have considerable amounts of CAA, which correlates with our in vitro fibrinogen binding experiments.

Oligomeric Aβ42 interacts with fibrinogen with high binding affinity (15, 16, 18), more so than fibrillar Aβ42. Given the importance of soluble oligomeric Aβ in AD pathology (20, 21), our SPR fibrinogen binding results (Fig. 1 *B* and *C*) and the clot structural effects (Fig. 2) demonstrated by HCAA Aβ oligomers further corroborate that the oligomeric state of Aβ is important in its interaction with fibrin(ogen) (15). Therefore, we also analyzed oligomeric Aβ species in HCAA brains (Fig. 5) using an Aβ oligomer-specific antibody (NAB61) (26). While HCAA brains exhibited higher levels of CAA pathology (Fig. 4*A*), they did not exhibit higher total Aβ deposits compared to EOAD brains (Fig. 4*C*), due to their abundant parenchymal Aβ plaques. However, HCAA brains contained much higher levels of vascular Aβ oligomers (Fig. 5*A*, NAB61, green) compared to the EOAD brains, which was confirmed with our quantification (Fig. 5*B*). Confocal imaging showed abundant fibrin(ogen) colocalized with Aβ oligomers in HCAA-Dutch and -Iowa brains, depicted as an overlapping merged channel (Fig. 5*A*, merged, yellow) particularly at sites of CAA pathology. Quantification showed higher levels of Aβ oligomer-fibrin(ogen) colocalization in HCAA-Dutch brains compared to EOAD brains (Fig. 5*C*). Furthermore, NAB61-positive (+) vessels also revealed much higher levels of intra- and extravascular fibrin(ogen) deposition in HCAA brains compared to EOAD brains (Fig. 5*D*). These findings provide evidence that the vast presence of vascular Aβ in CAA pathology in HCAA brains might be composed of a mixture of highly aggregated and oligomeric Aβ, both of which may be abundantly codepositing with fibrin(ogen) along cerebral vessels. The higher presence of Aβ oligomers at sites of CAA pathology in HCAA patients' brains compared to in EOAD brains may be attributable to the stronger interaction between mutant HCAA Aβ oligomers and fibrin(ogen) compared to WT Aβ, which can greatly contribute to their vascular deposition.

To aid the visualization of the codeposited/colocalized fibrin (ogen) and Aβ deposits (the Congo Red probe) or Aβ oligomers (the NAB61 probe) in HCAA patient brains, close-up confocal z-stack images of CAA-laden vessels were obtained (*SI Appendix*, Fig. S5). The z-stack images were compiled into three-dimensional movies that allow close inspection of the vascular Aβ-fbg colocalization (Movies S1–S8). CAA-laden vessels in the HCAA-Dutch and EOAD group brains were selected by identifying vessels with abundant vessel Congo Red signal or NAB61 signal. HCAA-Dutch and -Iowa brain samples contained abundant vascular fibrin(ogen) within and around cerebral vessel walls, often colocalizing and/or near aggregated Aβ (*SI Appendix*, Fig. S5*A*) and Aβ oligomers (*SI Appendix*, Fig. S5*B*) at various depths of tissue, whereas EOAD patient samples contained much less codeposited fibrin(ogen) at sites of CAA.

To ensure we were assessing vascular Aβ and fibrin(ogen) across similarly sized vessels across HCAA-Dutch, EOAD, and ND brains, we further stratified our IF analyses of levels of fibrin(ogen), congophillic Aβ, and Aβ oligomer by separate vessel sizes (*SI Appendix*, Fig. S6). We quantified the percent area of target protein contained in the vessel walls of larger vessels, which included medium to larger arterioles, and smaller vessels, consisting of arterioles, capillaries, and venules. In HCAA-Dutch brains, larger vessels had increased levels of vascular fibrin(ogen) (*SI Appendix*, Fig. S6*A*), Aβ oligomer deposits (*SI Appendix*, Fig. S6*C*), and fibrin(ogen) colocalization with congophillic Aβ (*SI Appendix*, Fig. S6*D*) and Aβ oligomers (*SI Appendix*, Fig. S6*E*) compared to in EOAD. HCAA-Dutch brain small vessels also contained higher

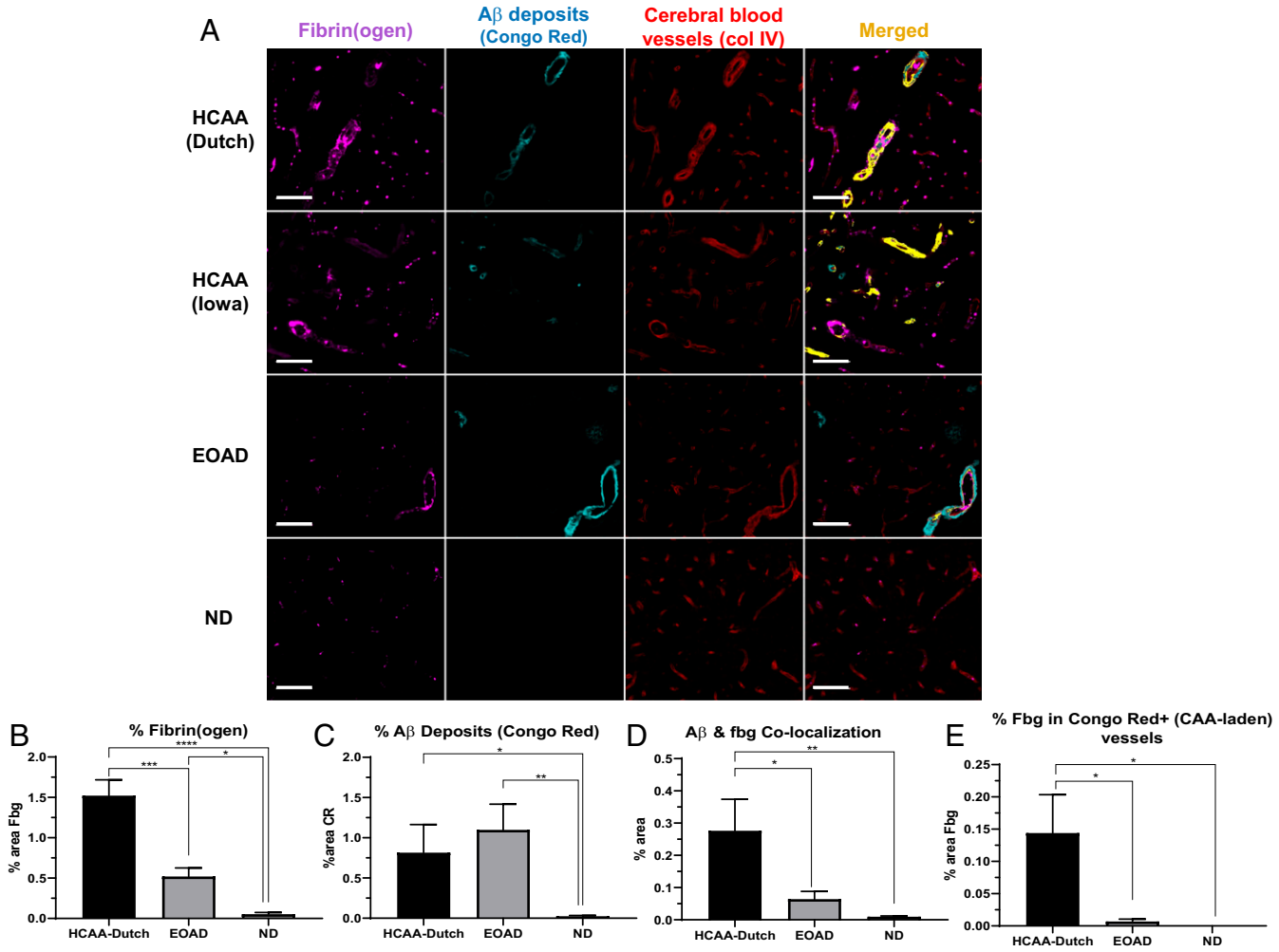

Fig. 4. Increased fibrin(ogen) deposits and Aβ-fibrino(gen) codeposition in HCAA patients' occipital cortex. Representative 20× images of brain sections were probed with antibodies against fibrin(ogen) (fbg, magenta), congophillic Aβ deposits using Congo Red dye (CR) (cyan), and blood vessels (col IV, red). (*A*) Occipital cortical sections in HCAA-Dutch ($n = 5$) and -Iowa ($n = 1$) type patient brains show abundant intra- and extravascular fibrin(ogen) deposits (magenta) and high amounts of vascular Aβ (cyan) around cerebral blood vessels (red), demarcated by basement membrane collagen IV, which frequently overlapped (Merged, yellow) at sites of CAA. (*B* and *C*) Quantification of percent area of target protein reveals elevated levels of fibrin(ogen) and Aβ deposits, respectively. (*D* and *E*) Confocal analysis shows elevated colocalization between Aβ and fibrin(ogen) in HCAA-Dutch brains, with particularly higher levels of fibrin(ogen) codeposition in CAA-laden vessels (Congo Red-positive), compared to EOAD ($n = 5$) and ND ($n = 7$) brains. Due to the limited amount of HCAA-Iowa ($n = 1$) individuals available in our study, it was not included in our IF quantification analysis. Statistical analyses were performed using one-way ANOVA followed by Tukey's post hoc test. ****$P < 0.0001$; ***$P < 0.001$; **$P < 0.01$; *$P < 0.05$. (Scale bars: 100 μm.)

levels of fibrin(ogen) deposits (*SI Appendix*, Fig. S6*F*), Aβ oligomers (*SI Appendix*, Fig. S6*H*), and Aβ oligomers-fbg colocalization (*SI Appendix*, Fig. S6*J*). We excluded quantification of large blood vessels, including small arteries, greater than 250 μm in diameter because large blood vessels were unevenly distributed between samples.

To further examine possible differences in vessel distribution in the patient brain samples, we analyzed vessel density (vessel count per square millimeter) (*SI Appendix*, Fig. S7*A*) and percent collagen IV (*SI Appendix*, Fig. S7*B*) area, an indicator of vessels' sizes. There was no statistical difference in vessel density among the three patient groups although EOAD and ND brains trended higher in density. There was also no statistical difference in vessel area or sizes (percent collagen IV) among the groups although HCAA-Dutch brain samples trended higher, with frequent larger caliber vessels.

Discussion

Here, we report high levels of mutant Aβ-fibrin(ogen) codeposition in HCAA-Dutch and -Iowa patient postmortem occipital brain tissue, especially at cerebral blood vessel sites with a high burden of CAA pathology, which may be explained by stronger interaction between HCAA Aβ and fibrinogen. Our in vitro findings show that the presence of Dutch- and Iowa-mutant Aβs leads to the formation of fibrin clots that are more structurally altered and more resistant to plasmin-mediated fibrinolysis compared to WT Aβ-induced clots. These findings may be explained by the fact that mutant Dutch- and Iowa-Aβ42 and -Aβ40 have stronger binding affinities to fibrinogen compared to both WT Aβ42 and WT Aβ40.

The increased binding affinity between HCAA Aβs and fibrinogen could be explained by the increased aggregation propensity featured by the mutant Aβs and/or the HCAA-linked amino acid substitutions. Our assessment whether an increased aggregated state in Aβ would increase its binding to fibrinogen (*SI Appendix*, Fig. S2) indicated that an aggregated Aβ42 peptide with a more proto-fibrillar structure (*SI Appendix*, Fig. S2*B*) did not have an increased binding affinity to fibrinogen compared to less aggregated Aβ42 (*SI Appendix*, Fig. S2 *A* and *D*). In addition,

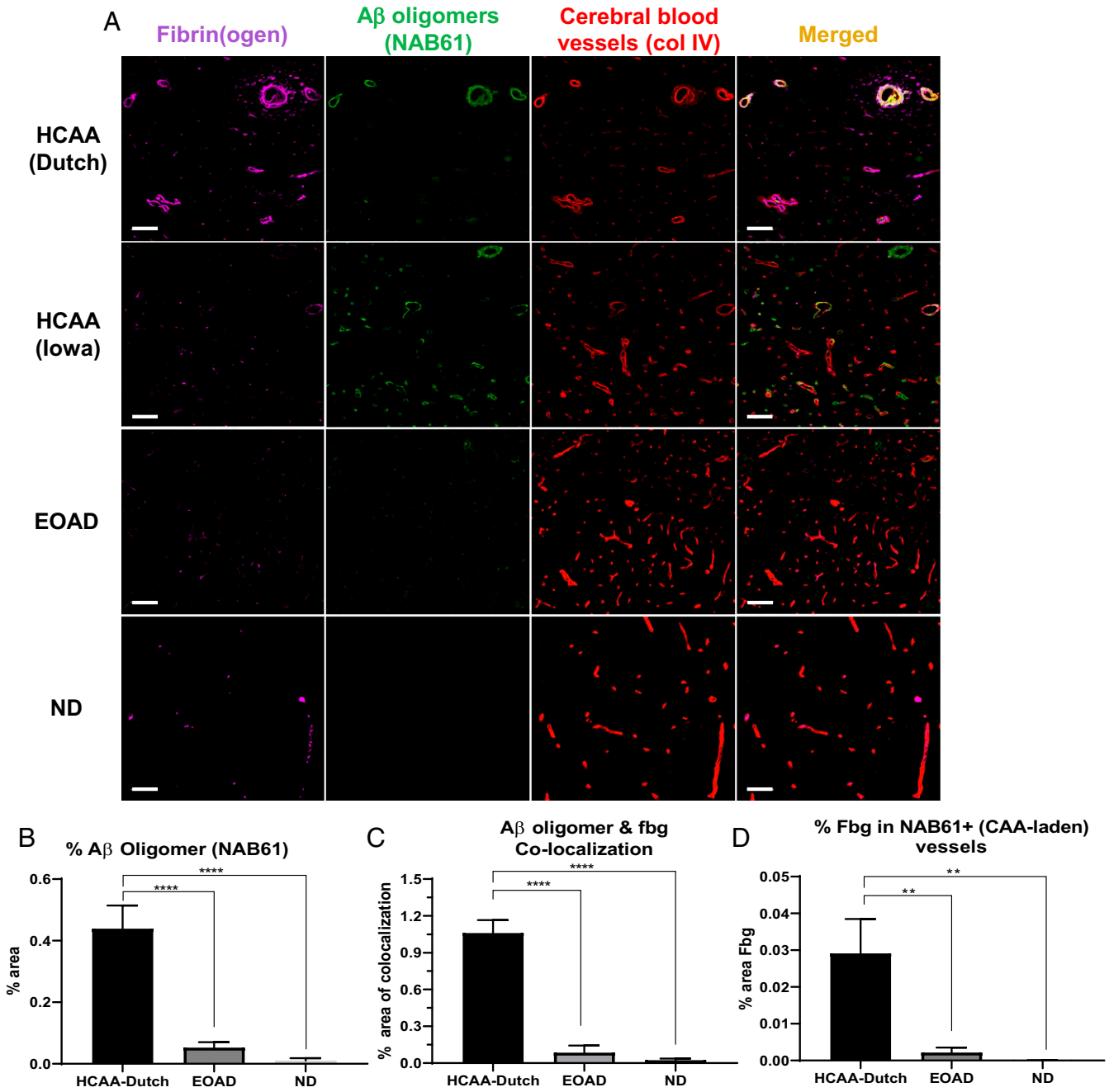

Fig. 5. Increased cerebrovascular Aβ oligomer and fibrin(ogen) codeposition in HCAA patients' cortical blood vessels. Representative 20× images of brain sections were probed for fibrin(ogen) (fbg, magenta), Aβ oligomers (NAB61, green), and blood vessels (col IV, red). (*A*) Brain sections from HCAA-Dutch ($n = 5$) and -Iowa ($n = 1$) patients show extensive Aβ oligomer deposits abundantly colocalizing (merged, yellow) with intra- and extravascular fibrin(ogen) along cerebral blood vessel walls, most probably at sites of CAA pathology. The EOAD group demonstrated sparse NAB61 signal or Aβ oligomer deposits at sites of apparent parenchymal plaques. (*B*) Quantification of percent area of NAB61 signal reveals significantly elevated levels of Aβ oligomer deposition, in HCAA-Dutch brain compared to EOAD ($n = 5$) and ND ($n = 5$) brains. (*C* and *D*) Colocalization analysis of the same tissue sections using confocal microscopy reveals dramatic colocalization between Aβ oligomers and intra- and extravascular fibrin(ogen) in HCAA-Dutch brains compared to the EOAD and ND groups, which was particularly prominent along cerebral vessel walls. There was almost no colocalization between fibrin(ogen) and Aβ oligomers at sites of parenchymal plaques throughout the three patient groups. Due to the limited amount of HCAA-Iowa ($n = 1$) individuals available in our study, it was not included in our IF quantification analysis. Statistical analyses were performed using one-way ANOVA followed by Tukey's post hoc test. $^{****}P < 0.0001$; $^{**}P < 0.01$. (Scale bars: 100 μm.)

our SPR fibrinogen binding results for Dutch40 and Iowa40 (Fig. 1 *H* and *I*) further drive the point that differences alone in the aggregation state of Aβ are not enough to dictate fibrinogen binding strength. Given that SPR response signal is known to be directly proportional to the change in bound analyte (Aβ) to the ligand (fibrinogen), the SPR response curves for Iowa40 were higher compared to Dutch40 (Fig. 1 *H* and *I*) at similar peptide concentrations most likely because Iowa40 aggregated into larger protofibrils compared to Dutch40 (*SI Appendix*, Fig. S2 *E* and *F*). However, Dutch40 and Iowa40 had comparable binding affinities to fibrinogen, 12 ± 2.4 nM and 6.8 ± 2.3 nM (Fig. 1*B*), respectively, that are not statistically different. Taken together, our results indicate that, while the aggregation state

of the HCAA Aβ or WT Aβ may have an influence in its binding affinity to fibrinogen, it seems that is it not the sole factor in determining fibrinogen binding strength. It is possible that the amino acid substitutions in the Dutch- and Iowa-Aβ peptides may have a larger influence in their interaction with fibrinogen.

The possible mechanisms through which HCAA Aβs perturb clot structure and fibrinolysis are the same as WT Aβ42's perturbation on clot structure and lysis (16). In non-HCAA AD patient cases, WT Aβ42 contributes to cerebrovascular pathology and CAA formation and delays fibrinolysis by binding to two regions: the C terminus of the β-chain of fibrinogen near the b-hole (15), and to a region of the αC-region of fibrinogen (Aα239–421) (17). This αC region of fibrinogen is known to bind plasminogen and includes plasmin cleavage sites (27). The higher binding affinity of the mutant HCAA Aβ peptides to fibrin(ogen) may further impede plasminogen binding and access of tPA and plasmin(ogen) to fibrin clots, which can contribute to the increases in half-lysis times compared to WT Aβ (Fig. 3 *C* and *D*). Stronger binding to the region close to the b-hole of fibrinogen may further impair lateral aggregation of fibrin protofibrils (15) and can result in the observed Dutch- and Iowa-Aβ induced clot structures that are more irregular and have more gaps (Fig. 2), thus also lowering the maximal optical density (OD) as observed in the clot lysis kinetic curves (Fig. 3*B*).

Although Dutch- and Iowa-Aβ show similar interactions with fibrinogen, in terms of binding affinity (Fig. 1), effects on fibrin clot structure (Fig. 2), and effects on clot lysis (Fig. 3), there are nuanced differences between the mutant Aβ peptides that should be noted. Differences in clot structure induced by Dutch40 (Fig. 2*E*), compared to Iowa40's effect (Fig. 2*F*), include qualitatively different fibrin clumps with a rosette-like appearance, more aggregates, and thinner fibers (Fig. 2 *I* and *K*). Possible reasons for these differences in fibrin clot perturbation include differences in the Aβ aggregation profile and changes to the stoichiometry between WT and HCAA Aβ peptides for fibrinogen (16, 17). Our TEM analysis of the structure of the oligomeric and proto-fibrillar forms of Aβ peptides (*SI Appendix*, Fig. S3) shows that, while Iowa42 and Dutch42 peptides both have short proto-fibrillar forms, Dutch40 and Iowa40 peptides differ. Iowa40 peptide shows increased elongated proto-fibrils compared to Dutch40's aggregation pattern. Differences in aggregated peptide structures between Dutch40 and other Aβs could account for the differences in which they affect fibrin clot structure. In addition, HCAA mutant Aβs may have additional binding regions within fibrinogen and induce a different stoichiometry between Aβ and fibrinogen.

Our IF analysis of HCAA patient brains helped corroborate the physiological relevance of our in vitro findings showing stronger interactions between mutant HCAA Aβ, specifically their oligomeric form, and fibrinogen. While this strong interaction can occur throughout the brain, wherever there is CAA pathology, the brain area that we decided to compare among the three human groups (HCAA-Dutch, EOAD, and ND) was the occipital cortex. Occipital brain tissue was selected based on the known predilection of CAA for posterior regions: in particular, the occipital lobe (22, 25). This occipital localization is found in both sporadic CAA patients and in AD patients with concurrent CAA, with increasing occipital vascular involvement with increasing AD pathology (22). In the case of HCAA, vascular deposits also start in the occipital lobe, but, in advanced cases, all brain regions are involved (5, 11).

Our analysis of Aβ and fibrin(ogen) colocalization in human HCAA patient brains highlight the role the aggregated state of Aβ has in AD vascular pathology. In our analysis, the use of Congo Red detected highly aggregated and congophillic Aβ at Aβ parenchymal plaques and CAA sites in HCAA and EOAD patients; however, there was no distinction in Aβ deposit levels between the two groups (Fig. 4*C*). In contrast, by using NAB61, we were able to reveal much higher levels of Aβ oligomers in HCAA-Dutch brains compared to EOAD brains, especially at sites of CAA (Fig. 5*B*).

Further stratification of our IF analyses based on vessel size indicated that there were different patterns of congophillic Aβ deposits in HCAA-Dutch and EOAD brains across larger (*SI Appendix*, Fig. S6 *A–E*) and smaller (*SI Appendix*, Fig. S6 *F–J*) vessels. In HCAA-Dutch brains, smaller vessels contained much lower congophillic Aβ deposits (*SI Appendix*, Fig. S6*G*) compared to EOAD brains, which is characteristic of HCAA-Dutch CAA pathology (28). EOAD brains also contained abundant CAA-laden large and small vessels with aggregated Aβ deposits (*SI Appendix*, Fig. S6 *B* and *G*), which is in agreement with the high incidence of CAA pathology in AD patients (2). These differences in Aβ deposit patterns based on vessel size reflects the existence of substantial CAA pathology in both patient groups, with the added caveat that HCAA Dutch-type CAA is mostly restricted to the arterioles (28). Although NAB61 was also able to detect parenchymal plaques in HCAA-Dutch and EOAD brains, its specificity in detecting vascular Aβ oligomers, including in larger (*SI Appendix*, Fig. S6*C*) and smaller (*SI Appendix*, Fig. S6*H*) vessels, highlighted the role cerebrovascular mutant Aβ oligomers have in their interaction and codeposition with fibrin(ogen) along cerebral vessel of various sizes (*SI Appendix*, Fig. S6 *E* and *J*). Furthermore, while smaller vessels in EOAD brains had noticeable levels of congophillic Aβ (*SI Appendix*, Fig. S6*G*) and Aβ oligomer (*SI Appendix*, Fig. S6*H*), fibrin(ogen) colocalization with Aβ oligomer (*SI Appendix*, Fig. S6*J*) was significantly lower compared to HCAA-Dutch brains. These results are in agreement with our previous in vitro binding experiments revealing that there is a strong binding affinity between oligomeric Aβ, especially mutant oligomeric HCAA Aβs as observed in our SPR binding experiments (Fig. 1), and fibrin(ogen), but weak binding between fibrin(ogen) and Aβ aggregates.

Taken our results together, it seems that mutant oligomeric HCAA Aβ may be interacting and binding with vascular fibrin(ogen) with high affinity in and around cerebral blood vessels, which can lead to their codeposition. The abundance of HCAA Aβ oligomers and fibrin(ogen) codepositing in HCAA patients' cerebrovasculature can lead to HCAA Aβ-induced clots that are severely structurally abnormal and resistant to fibrinolysis. Therefore, these findings suggest there could be persistent HCAA Aβ-fibrin(ogen) along cerebral vessels, which can greatly contribute to the exacerbated CAA pathology observed in HCAA disease.

The persistence of fibrin(ogen) in CAA-laden vessels can bring about severe local proinflammatory changes (29, 30), which can contribute to vascular pathology in HCAA. Due to the potential cross-talk between coagulation and inflammation (31), it is difficult to discern what pathways or mechanisms contribute to specific vascular pathologies in HCAA that include CAA and hemorrhagic strokes. Aβ's partner in CAA deposition, fibrin, the cleaved form of fibrinogen, plays a major role in plasminogen activation by stimulating the initial conversion of plasminogen into plasmin and further enhancing the rate of reaction (27). However, fibrin may not be the sole contributor to plasminogen activation. Fragments of Aβ containing the Dutch mutation and other fibrillar Aβ peptides have been observed to enhance tPA-mediated plasminogen activation in vitro (32, 33). If that were the case, a structurally altered clot with codeposited fibrin(ogen)/HCAA Aβ that is resistant to plasmin-mediated degradation, as shown by our in vitro findings, could be dramatically enhancing the proteolytic activity of tPA and plasmin(ogen), both principal mediators of fibrinolysis. Alterations to the proteolytic system may be contributing to a local hemorrhagic environment where proteolytic amplification could lead to focal degeneration of the vessel wall. Recent RNA sequencing studies using postmortem HCAA-Dutch patient brain tissue has shown up-regulation of *SERPINE1* (PAI-1) and *SERPING* (C1-inhibitor) (34), both of which play major roles in regulating aspects of hemostasis. Alterations to key regulators of fibrinolysis could be occurring in

response to codeposited fibrin(ogen)/HCAA Aβ in the vascular wall and deserves further investigation.

Our present study advances the understanding of the etiology behind one of HCAA's main cerebrovascular pathologies and suggests a role for fibrin(ogen) and mutant HCAA Aβ oligomers in this disease. Our findings suggest the amino acid mutations in the HCAA Aβ peptides increase the interaction between deposited Aβ and fibrin(ogen) along the cerebrovasculature in vivo. While likely not the sole contributor, the stronger interaction could be a driver of the formation of the exacerbated CAA found in HCAA.

Materials and Methods

Preparation of WT Aβ, HCAA Mutant-Type Aβ Peptides, and Fibrinogen. WT and HCAA mutant, Dutch- and Iowa-type, Aβ42 and Aβ40 peptide (Anaspec or Bachem) oligomers were prepared following established protocols (35), with the exception that, for SPR assays, the peptides were reconstituted in 5% dimethyl sulfoxide (DMSO) in phosphate-buffered saline (PBS) (pH 7.4) instead of 5% DMSO in 50 mM Tris·HCl (pH 7.4). Purified human fibrinogen (EMD Millipore) was prepared in PBS (pH 7.4) for SPR experiments and in 50 mM Tris·HCl (pH 7.4) for clot turbidity assays and for clot formations viewed under ScEM. For SPR experiments, fibrinogen was prepared in the following manner: 1) biotinylated using the Sulfo-NHS-LC-Biotin kit (Thermo Scientific) with 10-fold molar excess of biotin reagent resulting in one to three biotin groups per molecule of fibrinogen, and 2) desalted and removed of excess biotin using Zeba Spin Desalting Columns (Thermo Scientific). Aβ peptides, fibrinogen, and biotinylated-fibrinogen were diluted to desired concentrations with the same reconstitution buffer. Concentrations for these peptides were established by bicinchoninic (BCA) assay (Thermo Scientific).

Probe of Aβ–Fibrin(ogen) Interaction in Fibrinogen-Binding Central Region of Aβ Using AlphaLISA Assay. Four alanine-scanning peptide analogs of Aβ (L17A, E22A, D23A, and V24A) were synthesized by replacing L17, E22, D23, and V24 in Aβ42 with alanine and subsequently biotinylated at the N terminus (Chinese Peptide Company). Various concentrations (0.01 to 20 mM) of these alanine-scanning Aβ42 peptide fragments were incubated with 1 nM fibrinogen for 30 min at room temperature in a final volume of 10 mL of assay buffer (25 mM Tris·HCl, pH 7.4, 150 mM NaCl, 0.05% Tween 20, 0.1% BSA) in white 384-well plates (Greiner). The mixture was incubated with the anti-fibrinogen antibody, 20 mg/mL streptavidin-conjugated donor, and protein A-conjugated acceptor beads (PerkinElmer) for 90 min at room temperature. Samples were read by a PerkinElmer EnVision plate reader.

Examination of Aβ Binding to Fibrinogen Using SPR Analysis. SPR experiments were performed to determine the binding affinity (K_D) of WT and HCAA mutant Aβ peptides to fibrinogen. The SPR Bio-Rad ProteOn XPR36 instrument was able to generate association (k_a) and dissociation (k_d) rate constants for the biomolecular binding interactions between individual analytes (the various Aβ peptides) and the ligand, biotinylated-purified human fibrinogen (final 0.5 mg/mL), immobilized on a ProteOn NLC sensor chip containing a NeutrAvidin layer for binding biotin-labeled molecules. The various Aβ peptides were each diluted to various concentrations (Fig. 1) using PBS with 0.005% Tween 20 (PBST) as running buffer (final 0.5% DMSO-PBST). They were injected for 2 min at a rate of 30 μm/min for the association phase. After the dissociation phase, the SPR chip was rinsed with 1 M NaCl and 50 mM NaOH. Corresponding 0.5% DMSO-PBST dilutions were used as a buffer blank. The k_as and k_ds for each analyte interaction with fibrinogen were used to calculate the equilibrium dissociation constant ($-K_D$). The SPR instrument is available at The Rockefeller University High Throughput Screening Resource Center.

Examination of In Vitro Fibrin Clot Fibrinolysis and Clot Structure. Clot turbidity assays to assess the functional impact of the various Aβ peptides on clot formation and dissolution (clot lysis) were performed at room temperature in high binding 96-well plates (Fisher Scientific) using a Spectramax Plus384 reader (Molecular Devices). Clot formation and lysis involved first incubating fibrinogen (1.5 μM) without or with the individual Aβ oligomers (3 μM) and purified human plasminogen (final 250 nM; purified from human plasma in the S.S. laboratory) for 20 min. To induce fibrin formation and subsequent lysis, thrombin (0.75 U/mL), $CaCl_2$ (5 mM), and purified human tPA (final 1 nM) in 20 mM 4-(2-hydroxyethyl)-1-piperazineethanesulfonic acid (Hepes) buffer (pH 7.4) with 137 mM NaCl in a volume of 200 μL was mixed in. As fibrin forms due to thrombin activity, tPA activity is enhanced, leading to the activation of plasminogen into plasmin, which then subsequently starts degrading the fibrin clot. Clot formation and dissolution were monitored by measuring the changes in turbidity (OD) at 350 nm over time, reading at 30-s intervals. Fibrin clot lysis rates were compared using half-lysis times, which were calculated from the time when max OD was achieved to the time when the clot reached half its maximum turbidity after OD started decreasing.

To view fibrin clots using ScEM, clots were formed using fibrinogen (1.5 μM or 1 μM) on round glass coverslips at room temperature. Fibrinogen was incubated in the absence or presence of the various Aβ peptides (WT and HCAA mutant-type Aβ; each at final 3 μM or 0.375 μM) oligomers for 20 min at room temperature. Fibrin clots were induced with the addition of thrombin (0.75 U/mL), $CaCl_2$ (5 mM), 137 mM NaCl in 20 mM Hepes (pH 7.4). One hour after adding thrombin, clots were gently washed twice with cold sodium cacodylate buffer (0.1 M) for 2 min each time and fixed with 2% glutaraldehyde on ice for 30 min. After ascending serial dehydration with ice cold ethanol (20 to 100%), the fibrin clots on the glass coverslips were sputter-coated with gold palladium. Images were obtained using Leo 1550SEM at the Electron Microscopy Resource Center (EMRC) at The Rockefeller University and the Gemini300SEM at New York University Langone Health (NYULH), operating at 4.0 kV and using SmartSEM software.

ImageJ (NIH) software was used for structural analysis of fiber diameter and number of clot aggregates and clumps present with the various Aβ peptides tested used. Three images per clot at a pixel size of 14.3 nm (fibrin alone and Aβ-induced clot) were used for quantification. The diameters of six fibers at five nonoverlapping regions for each clot were measured. Clumps were qualitatively defined and chosen by selecting fiber conjunctions that contained six or more intersecting fibers. The clumps were usually concentrically amorphous in shape. Publication figures were assembled using Image J software.

Patient Brain Tissue Samples. Postmortem tissue samples were obtained from various sources and were requested to derive from patients that are age-matched, specifically from the occipital cortical region, and for sections to be processed as described in *Brain Tissue Processing* (see *SI Appendix*, Table S1 for a list of patient characteristics and more tissue information). HCAA patient brain tissue was derived from nonhemorrhagic regions and, in all cases, was derived from the occipital lobe contralateral to the lethal stroke leading to or contributing to the patient's death. The EOAD group consisted of patients affected by early-onset AD phenotype and confirmed by postmortem analysis. EOAD patient in our analysis do not contain any mutation within Aβ or near Aβ cleavage site as we confirmed by sequencing of exon 16 and 17 of the APP gene. Brain tissue from an HCAA Iowa-type patient was limited due to very scarce availability. Out of four reported Iowa cases reported on PubMed, only one was available. One Iowa patient brain tissue was obtained through collaboration with Michael A. Farrell (Beumont Hospital, Dublin, Ireland). HCAA Dutch-type patients' ($n = 5$) tissue sections were obtained from Leiden University Medical Center (Leiden, The Netherlands) from five different individuals. Collectively, the HCAA group consisted of six individual patients ($n = 6$, three male, three female, age 53 ± 1 y, postmortem interval [PMI]/autolysis time of 9 ± 3 h, mean ± SEM). EOAD and control non-AD (ND) human tissue was obtained from the NIH NeuroBioBank's Brain and Tissue repository at the University of Maryland (Baltimore, MD) and from the repository at the Veterans Affairs (VA) Greater Los Angeles (LA) Healthcare System. Collectively, the EOAD group consisted of five individuals ($n = 5$, two male, three female, age 58 ± 1 y, PMI/autolysis time of 12 ± 2 h, mean ± SEM). Collectively, the ND group consisted of seven individuals ($n = 7$, four male, three female, age 58 ± 1 y, PMI/autolysis time of 16 ± 2 h, mean ± SEM).

Brain Tissue Processing. Human HCAA-Dutch and -Iowa, EOAD, and control (ND) brain sections were obtained and processed by the following manner: fixed in 20% formalin, paraffin-embedded, sectioned at 5 μm thickness, except for HCAA-Iowa tissue, which was sectioned at 4 μm thickness. For IF analysis, these brain sections were deparaffinized using CitriSolv (Decon Labs) and rehydrated serially with descending ethanol concentrations (100 to 70%) and then treated with proteinase K (Dako) before performing the staining protocol listed above.

Antibodies and IF. The following primary antibodies were used for HCAA, EOAD, and ND patient cortical brain IF probe for fibrin(ogen), Aβ plaques/deposits, and Aβ oligomer staining: goat polyclonal anti-collagen IV (1:200; EMD Millipore) antibody, rabbit polyclonal anti-fibrin(ogen) (1:800; Dako) antibody, mouse monoclonal anti–Aβ-oligomer antibody "NAB61" (1:200; Virginia Lee's laboratory, University of Pennsylvania, Philadelphia, PA) (26).

Brain sections were initially blocked for 1 h with 2% donkey:horse serum (1:1) and then incubated in each of the primary antibodies overnight at 4 °C. The following day, sections were incubated with the following fluorescent secondary antibodies and dyes: fluorescent secondary antibodies corresponded to the primary antibody using either Alexa Fluor 350 or 555 for donkey anti-goat (for anti-collagen IV antibody), Alexa Fluor 488 anti-mouse (for NAB61), and Alexa Fluor 488 or 647 donkey anti-rabbit (for anti-fibrin [ogen]). Next, Aβ deposits or plaques were visualized with 0.2% Congo Red in 70% 2-propanol and subsequently counterstained with 0.3% Sudan Black B in 70% ethanol to reduce lipofuscin green autofluorescence. Sections were then covered with Vectashield (Vector Labs) and mounted on glass slides and imaged.

Image Acquisition and Processing. Following immunostaining, our Aβ and fibrin(ogen) colocalization analyses of the patient brain sections were imaged with laser scanning microcopy using an Inverted Zeiss Axio Observer Z1 confocal microscope (ZEISS) (Bio-Imaging Resource Center, The Rockefeller University). Two large sections per patient sample were used for quantifying the staining. We captured two nonoverlapping 8 × 8 tiled images at 20× for every sample for analysis. We probed for fibrin(ogen) and Aβ using Congo Red staining and the NAB61 probe in two separate sets of tissue sections. Then 405-nm, 488-nm, and 633-nm confocal laser lines were used to view fluorescent secondary antibodies and the Congo Red dye signal. Stitched (20% overlap) 8 × 8 tiled images for every patient section were captured with Zen Black software (ZEISS) using a 20.0× water objective to view as much tissue as possible for analysis.

Digital Image Analysis for Cortical Fibrin(ogen), Aβ Deposits (Plaques), and Aβ Oligomer Quantification. For percent analysis of fibrin(ogen), collagen IV, NAB61, and Aβ signal, patient brain sections that were immunostained and imaged with confocal microscopy were analyzed using NIS-Elements Advanced Research software suite version 5.1 (Nikon). Each multichannel red, green, and blue (RGB) image was analyzed by processing each of its single RGB channels (red, blue, green). Each channel was thresholded to collect the total number of pixels with numeric values inside the thresholded interval, which was then converted to a binary layer. The binary layer provided the total area of positive staining as a percentage of total image area. Data indicating percent area of immunofluorescent targets [e.g., % fibrin(ogen)] were organized into graphs using Prism 8 (GraphPad Software, San Diego, CA); one-way ANOVA, followed by Tukey's multiple comparisons post hoc test, was performed using GraphPad Prism version 8.0.0 for Windows. For colocalization analysis of images captured with confocal microscopy, 8 × 8 tile images were thresholded using ImageJ (NIH). Publication figures were assembled using Image J software.

For analyses indicating percent area of target [e.g., % fibrin(ogen)] based on vessel size, the collagen IV channel in the Congo Red probe and NAB61 probe was size-thresholded in the following manner: For selection of "larger vessels," the size threshold was set to include only objects 20 to 250 μM in size whereas "smaller vessels" were size-thresholded to include objects between 5 and 20 μM in size. We excluded large blood vessels greater than 250 μm in diameter because large blood vessels were unevenly distributed between samples.

Statistical Analysis. Bar graphs for publication were created using GraphPad Prism 8 (GraphPad Software, San Diego, CA). Statistical analyses were conducted using Prism 8. All numerical values presented in graphs are mean ± SEM. Statistical analyses were assessed as described in the text using either one-way ANOVA followed by Tukey's multiple comparisons test or two-tailed unpaired *t* test. *P* values below 0.05 were considered significant. *P* values were as follows: $****P < 0.0001$; $***P < 0.001$; $**P < 0.01$; $*P < 0.05$, and ns, not significant. Bar graphs of AlphaLISA, SPR, and in vitro turbidity experiments represent mean ± SEM of ≥3 separate experiments.

Data Availability. All data are available in the main text, *SI Appendix*, and Movies S1–S8.

ACKNOWLEDGMENTS. This work was supported by NIH Grants NS104386 (to H.J.A.) and NS10668 (to E.H.N. and S.S.), the Cure Alzheimer's Fund, the Alzheimer's Association, the Rudin Family Foundation, and John A. Herrmann, Jr. S.A.C. was supported by a Medical Scientist Training Program grant from the National Institute of General Medical Sciences of the NIH under Award T32GM007739 to the Weill Cornell/Rockefeller/Sloan Kettering Tri-Institutional MD–PhD Program. L.v.d.W was supported by The Netherlands Organization for Scientific Research (NWO, The Hague, The Netherlands), under research program VIDI, Project 864.13.014. Microscopy assistance at NYULH is a microscopy shared resource supported by Cancer Center Support Grant P30CA016087, and Gemini300SEM was purchased with support of NIH Grant S10 OD019974-01A1. We thank members of the S.S. laboratory for scientific discussion, particularly Dr. Hanna Berk-Rauch for her technical and experimental support, and Jonah Vernejoul for human postmortem tissue preparation. We also thank The Rockefeller University's Bio-Imaging Resource Center, EMRC, and High Throughput Screening Resource Center for assistance and access to experimental equipment and technical support. We also thank Drs. Kunihiro Uryu and Nadine Soplop for their expert help in electron microscopy. We acknowledge Dr. Alice Liang and Joseph Sall for assistance with ScEM work at the NYULH Division of Advanced Research Technologies (DART) Microscopy laboratory. We are thankful to the NIH NeuroBioBank, VA Greater Los Angeles Healthcare System, and University of Maryland brain banks for providing EOAD and ND patient brain tissues. We thank Dr. Michael Farrell (Beumont Hospital, Dublin, Ireland) for providing the scarce and precious human HCAA-Iowa brain tissue sections used for this study.

1. A. Viswanathan, W. A. Rocca, C. Tzourio, Vascular risk factors and dementia: How to move forward? *Neurology* **72**, 368–374 (2009).
2. A. Serrano-Pozo *et al*., Examination of the clinicopathologic continuum of Alzheimer disease in the autopsy cohort of the National Alzheimer Coordinating Center. *J. Neuropathol. Exp. Neurol.* **72**, 1182–1192 (2013).
3. S. Lee *et al*.; Dominantly Inherited Alzheimer Network, White matter hyperintensities are a core feature of Alzheimer's disease: Evidence from the dominantly inherited Alzheimer network. *Ann. Neurol.* **79**, 929–939 (2016).
4. Y. Iturria-Medina, R. C. Sotero, P. J. Toussaint, J. M. Mateos-Pérez, A. C. Evans; Alzheimer's Disease Neuroimaging Initiative, Early role of vascular dysregulation on late-onset Alzheimer's disease based on multifactorial data-driven analysis. *Nat. Commun.* **7**, 11934 (2016).
5. M. Yamada, Cerebral amyloid angiopathy: Emerging concepts. *J. Stroke* **17**, 17–30 (2015).
6. A. Viswanathan, S. M. Greenberg, Cerebral amyloid angiopathy in the elderly. *Ann. Neurol.* **70**, 871–880 (2011).
7. Y. D. Reijmer, S. J. van Veluw, S. M. Greenberg, Ischemic brain injury in cerebral amyloid angiopathy. *J. Cereb. Blood Flow Metab.* **36**, 40–54 (2016).
8. E. Auriel, S. M. Greenberg, The pathophysiology and clinical presentation of cerebral amyloid angiopathy. *Curr. Atheroscler. Rep.* **14**, 343–350 (2012).
9. S. X. Zhang-Nunes *et al*., The cerebral beta-amyloid angiopathies: Hereditary and sporadic. *Brain Pathol.* **16**, 30–39 (2006).
10. T. Revesz *et al*., Genetics and molecular pathogenesis of sporadic and hereditary cerebral amyloid angiopathies. *Acta Neuropathol.* **118**, 115–130 (2009).
11. M. Cortes-Canteli, D. Zamolodchikov, H. J. Ahn, S. Strickland, E. H. Norris, Fibrinogen and altered hemostasis in Alzheimer's disease. *J. Alzheimers Dis.* **32**, 599–608 (2012).
12. M. Cortes-Canteli, L. Mattei, A. T. Richards, E. H. Norris, S. Strickland, Fibrin deposited in the Alzheimer's disease brain promotes neuronal degeneration. *Neurobiol. Aging* **36**, 608–617 (2015).
13. J. C. de la Torre, Is Alzheimer's disease a neurodegenerative or a vascular disorder? Data, dogma, and dialectics. *Lancet Neurol.* **3**, 184–190 (2004).
14. J. Paul, S. Strickland, J. P. Melchor, Fibrin deposition accelerates neurovascular damage and neuroinflammation in mouse models of Alzheimer's disease. *J. Exp. Med.* **204**, 1999–2008 (2007).
15. H. J. Ahn *et al*., Alzheimer's disease peptide beta-amyloid interacts with fibrinogen and induces its oligomerization. *Proc. Natl. Acad. Sci. U.S.A.* **107**, 21812–21817 (2010).
16. D. Zamolodchikov, S. Strickland, Aβ delays fibrin clot lysis by altering fibrin structure and attenuating plasminogen binding to fibrin. *Blood* **119**, 3342–3351 (2012).
17. D. Zamolodchikov *et al*., Biochemical and structural analysis of the interaction between β-amyloid and fibrinogen. *Blood* **128**, 1144–1151 (2016).
18. M. Cortes-Canteli *et al*., Fibrinogen and beta-amyloid association alters thrombosis and fibrinolysis: A possible contributing factor to Alzheimer's disease. *Neuron* **66**, 695–709 (2010).
19. N. C. Alonzo, B. T. Hyman, G. W. Rebeck, S. M. Greenberg, Progression of cerebral amyloid angiopathy: Accumulation of amyloid-beta40 in affected vessels. *J. Neuropathol. Exp. Neurol.* **57**, 353–359 (1998).
20. B. DaRocha-Souto *et al*., Brain oligomeric β-amyloid but not total amyloid plaque burden correlates with neuronal loss and astrocyte inflammatory response in amyloid precursor protein/tau transgenic mice. *J. Neuropathol. Exp. Neurol.* **70**, 360–376 (2011).
21. I. Benilova, E. Karran, B. De Strooper, The toxic Aβ oligomer and Alzheimer's disease: An emperor in need of clothes. *Nat. Neurosci.* **15**, 349–357 (2012).
22. D. R. Thal, J. Walter, T. C. Saido, M. Fändrich, Neuropathology and biochemistry of Aβ and its aggregates in Alzheimer's disease. *Acta Neuropathol.* **129**, 167–182 (2015).
23. T. Wisniewski, J. Ghiso, B. Frangione, Peptides homologous to the amyloid protein of Alzheimer's disease containing a glutamine for glutamic acid substitution have accelerated amyloid fibril formation. *Biochem. Biophys. Res. Commun.* **180**, 1528 (1991).
24. D. M. Walsh, A. Lomakin, G. B. Benedek, M. M. Condron, D. B. Teplow, Amyloid beta-protein fibrillogenesis. Detection of a protofibrillar intermediate. *J. Biol. Chem.* **272**, 22364–22372 (1997).

25. P. K. Singh *et al*., Aminopyrimidine class aggregation inhibitor effectively blocks Aβ-fibrinogen interaction and Aβ-induced contact system activation. *Biochemistry* **57**, 1399–1409 (2018).
26. E. B. Lee *et al*., Targeting amyloid-beta peptide (Abeta) oligomers by passive immunization with a conformation-selective monoclonal antibody improves learning and memory in Abeta precursor protein (APP) transgenic mice. *J. Biol. Chem.* **281**, 4292–4299 (2006).
27. L. Medved, W. Nieuwenhuizen, Molecular mechanisms of initiation of fibrinolysis by fibrin. *Thromb. Haemost.* **89**, 409–419 (2003).
28. M. Maat-Schieman, R. Roos, S. van Duinen, Hereditary cerebral hemorrhage with amyloidosis-Dutch type. *Neuropathology* **25**, 288–297 (2005).
29. R. A. Adams *et al*., The fibrin-derived gamma377-395 peptide inhibits microglia activation and suppresses relapsing paralysis in central nervous system autoimmune disease. *J. Exp. Med.* **204**, 571–582 (2007).
30. D. Davalos *et al*., Fibrinogen-induced perivascular microglial clustering is required for the development of axonal damage in neuroinflammation. *Nat. Commun.* **3**, 1227 (2012).
31. M. Levi, T. van der Poll, H. R. Büller, Bidirectional relation between inflammation and coagulation. *Circulation* **109**, 2698–2704 (2004).
32. J. Davis, W. E. Van Nostrand, Enhanced pathologic properties of Dutch-type mutant amyloid beta-protein. *Proc. Natl. Acad. Sci. U.S.A.* **93**, 2996–3000 (1996).
33. I. B. Kingston, M. J. Castro, S. Anderson, In vitro stimulation of tissue-type plasminogen activator by Alzheimer amyloid beta-peptide analogues. *Nat. Med.* **1**, 138–142 (1995).
34. L. Grand Moursel *et al*., Brain transcriptomic analysis of hereditary cerebral hemorrhage with amyloidosis-Dutch type. *Front. Aging Neurosci.* **10**, 102 (2018).
35. W. B. Stine, L. Jungbauer, C. Yu, M. J. LaDu, Preparing synthetic Aβ in different aggregation states. *Methods Mol. Biol.* **670**, 13–32 (2011).